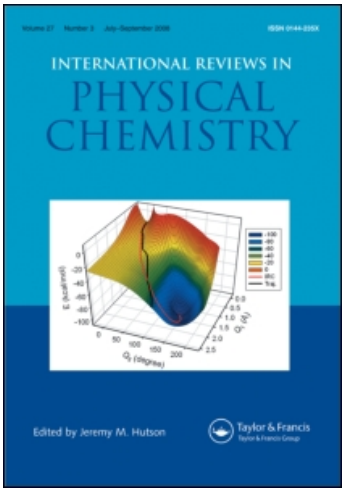

International Reviews in Physical Chemistry
Publication details, including instructions for authors and subscription information:
http://www.informaworld.com/smpp/title~content=t713724383

Complex formation and decay in ion-molecule reactions: Mode-selective scattering as a dynamical probe

Richard J. Green[a]; Scott L. Anderson[a]
[a] Chemistry Department, The University of Utah, Salt Lake City, UT, USA

Online publication date: 26 November 2010

To cite this Article Green, Richard J. and Anderson, Scott L.(2001) 'Complex formation and decay in ion-molecule reactions: Mode-selective scattering as a dynamical probe', International Reviews in Physical Chemistry, 20: 2, 165 — 188
To link to this Article: DOI: 10.1080/01442350118183
URL: http://dx.doi.org/10.1080/01442350118183

INT. REVIEWS IN PHYSICAL CHEMISTRY, 2001, VOL. 20, NO. 2, 165–188

Complex formation and decay in ion–molecule reactions: mode-selective scattering as a dynamical probe

RICHARD J. GREEN and SCOTT L. ANDERSON

Chemistry Department, 315 S. 1400 E. Rm. 2020, The University of Utah, Salt Lake City, UT 84112, USA

The potential energy surfaces for ion–molecule reactions typically have several minima that lie lower in energy than the asymptotes for the reactant and product channels. Such complexes can be covalently bound, hydrogen bonded or electrostatically bound. The nature of these complexes can have dramatic effects on the outcome of the reaction. We review three experimental studies that show three different cases of such influence. The reaction of acetylene cation with methane shows channels that proceed via a long-lived, covalently bound complex, and one channel that proceeds by a short-lived, weakly bound encounter complex. Specific reactant vibrations strongly influence both total reactivity and branching between the product channels, and the effect is related to the mode-specific coupling of vibration to the reaction coordinate. The reaction of phenol cation with ammonia is a case involving both electrostatically bound and hydrogen-bonded complexes, with ring-coordination complexes acting as precursors to the formation of the hydrogen-bonded complexes where reaction can occur. Again, vibration has a significant effect, related to the isomerization between coordination and hydrogen-bonded geometries. Finally, the reaction of ammonia cation with methanol involves competition between formation of different hydrogen-bonded intermediates, and the complex that forms largely determines the outcome of the reaction.

Contents

1. Introduction

A common feature of ion–molecule reactions is the existence of intermediate complexes that can mediate reaction, particularly at low collision energies where the

International Reviews in Physical Chemistry ISSN 0144-235X print/ISSN 1366-591X online © 2001 Taylor & Francis Ltd
http://www.tandf.co.uk/journals
DOI: 10.1080/01442350110034048

complex lifetimes can be long. There are three important classes of complexes. In reactions of unsaturated species, there are covalently bound complexes that can be bound by several electronvolts relative to both reactants and products. For collision energies up to a few electronvolts, such complexes can have lifetimes in the microsecond to nanosecond range—ample time to facilitate complicated rearrangements. In appropriate systems, hydrogen-bonded complexes exist, bound by 1–2 eV. These complexes also provide a pathway for hydrogen exchange and energy randomization, but not rearrangement of the heavy-atom skeleton. Finally, for many systems, there are electrostatic coordination complexes, typically bound by less than 1 eV. Even these weakly bound complexes can strongly influence reactivity and product branching at low collision energies. This paper reviews three reaction systems that demonstrate the effects that each type of complex can have. The dynamical consequences that might be expected from complex formation include increased collision time, enhanced (possibly selectively enhanced) energy randomization, reorientation of reactants into particular geometries, and control of product branching.

There are several approaches to studying ion–molecule reactions and these have been reviewed elsewhere [1–3]. The tool that we have developed for probing ion reaction dynamics is mode-selective differential scattering; that is, measuring both integral and differential cross-sections for the reaction of vibrationally mode-selected reactants. The initially selected reactant vibration tends to scramble early in collisions, because the intermolecular interaction perturbs bonding in the reactants, and the collision energy is wholly or partly converted to internal energy. As a consequence, mode-specific vibrational effects probe the early-time collision dynamics, including complex formation and energy randomization in weakly bound complexes. By following vibrational effects as a function of collision energy, it is often possible to infer changes in reaction mechanism with energy.

The recoil velocity distribution of scattered product ions provides several additional pieces of information. For reactions that take place on a time scale longer than a few picoseconds, rotation of the collision complex (on a picosecond time scale) results in isotropic product angular distributions. For reactions occurring on a shorter time scale, the velocity distribution often allows the preferred scattering mechanisms (e.g. stripping versus rebounding) and the collision time scale to be inferred. The recoil energy distribution provides insight into energy randomization in the collision and energy partitioning in the products. In particular, the degree of energy randomization often provides insight into complex lifetimes in the tens of picoseconds range, where direct information from the angular distribution is absent. When combined with techniques such as isotope labelling, *ab initio* calculations, and modelling of unimolecular rates; detailed mechanisms can be inferred for reactions taking place over millisecond to femtosecond time scales.

We have applied this technique to a variety of ion–molecule reaction systems, ranging in complexity from six to 20 atoms [4–20]. Zare and co-workers [21–25], Guettler [26] and Jones [27] have applied similar techniques to several reactions of NH_3^+ and NO^+, and Gerlich and co-workers [8, 28–30] have reported very detailed studies of a number of state-selected ion–molecule reactions, including work at subthermal collision energies. In addition, Ng and co-workers [31–33] have reported very detailed studies of the dynamics of H_2^+ and N_2^+ reactions, and Dutuit and co-workers [34–36] have examined state-selected $C_2H_2^+$ and $C_2H_4^+$ reactions, including some at very high levels of reactant excitation. Here we present results on three systems that illustrate the effects of each different type of intermediate complex.

2. Experimental and computational methodology and analysis

The experimental methodology has been described in detail previously [10–12, 14, 16]. Here we outline only the general procedures. The most difficult aspect of the method is preparing polyatomic cations with controlled excitation in different vibrational modes. Depending on the system, we have been successful with both resonance-enhanced multiphoton ionization (REMPI) and mass-analysed threshold ionization (MATI) [37]. The two methods are shown schematically in figure 1.

The general considerations for successful REMPI state selection have been outlined in a review [6]. In brief, the neutral precursor molecules are excited by one or more photons to an intermediate electronic state and then ionized by one additional photon. The resulting distribution of ion vibrational states depends on the properties of the intermediate state and cation ground state. In the simplest case, the intermediate is a Rydberg state—essentially a cation core, loosely coupled to the excited electron. As a consequence of the weak coupling, the molecular geometry is nearly identical with that of the free cation and, when the Rydberg state is ionized, the Franck–Condon principle favours leaving the cation in the same vibrational level that was populated in the Rydberg state. Ideally, ions can be produced in single and variable vibrational states, simply by tuning the REMPI laser to the appropriate vibrational levels of the Rydberg intermediate. In reality, the Rydberg states are often strongly mixed with nearby valence and Rydberg states, with disastrous consequences for state selection. To find suitable REMPI state selection routes, it is essential to measure the cation vibrational state distributions with photoelectron spectroscopy. Among polyatomics, suitable routes have been reported for acetylene [38, 39], OCS [40], NH_3 [21, 25] and acetaldehyde [41]. Very recently, we have discovered [42] that REMPI through the $3p_x$ state of formaldehyde can produce perfectly state-selected cations with up to 0.6 eV of vibrational energy, selectively placed in any of four different vibrational modes. The $C_2H_2^+$ and NH_3^+ systems discussed here are more typical, in that only two of the six possible modes can be selected by REMPI.

MATI state selection, used for the phenol work described below, is a more complex multiphoton ionization process than REMPI. The advantage is that, in principle, one has more control over the resulting ion vibrational state distribution. In MATI as used for our experiments, the molecule is single photon excited to an intermediate state and then excited with a second tunable laser to high Rydberg states converging on the desired cation vibrational state. A weak electric field (about 3 V cm^{-1}) is applied to reject any non-state-selected 'prompt' ions generated in the excitation process; then the high Rydberg states are field ionized by a stronger pulsed field (50 V cm^{-1}). In our experience, MATI and REMPI state selection are roughly complementary, MATI being best for molecules that can conveniently be excited by 1+1 photon schemes, and REMPI being most successful for 2+1 or 3+1 ionization stepping through higher-energy intermediate states.

The instrument is shown in figure 2, as set up for MATI. Ions are generated by MATI at the intersection of the laser and molecular beams. Prompt ion rejection and field ionization is carried out in a MATI source region 5 cm long; then the state-selected ions are injected into a rf quadrupole ion guide. For the REMPI experiments, the MATI source and quadrupole were replaced by a longer quadrupole guide, and ions were created inside the quadrupole. In either case, the focusing properties of the quadrupole guide are combined with time-of-flight (TOF) gating at the quadrupole exit, to generate a state-selected pulsed ion beam, with narrow energy spread. The ion beam is then injected into an octapole ion guide that guides the reactant ions through

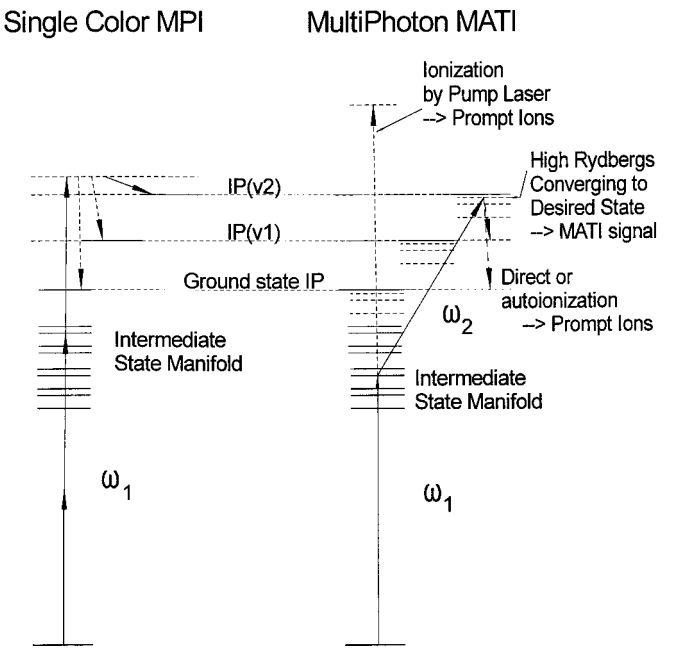

Figure 1. Diagrams of two methods of state-selective ionization: REMPI and mass-analysed threshold ionization.

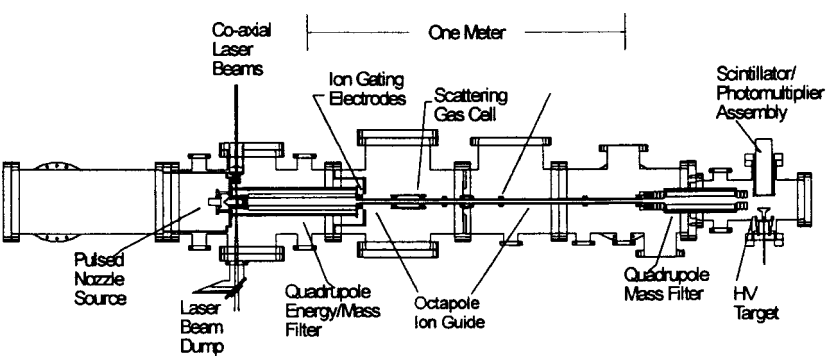

Figure 2. The guided ion-beam apparatus used in the studies reviewed here, as set up for MATI.

a scattering cell containing the neutral reactant at a pressure (about (3–7)$\times 10^{-5}$ Torr) low enough to ensure single-collision conditions. The octapole collects product ions, together with unreacted primary ions, and guides them to a quadrupole mass spectrometer for analysis. Integral cross-sections are calculated from ratios of reactant and product ions, together with the scattering cell pressure. TOF measurements of the reactant ion velocity distributions are used to calibrate the collision energy.

Two levels of detail can be achieved for the differential cross-section (i.e. product velocity distributions). Because the experiment is cylindrically symmetric about the octapole guide axis, the velocity distributions are also cylindrically symmetric. In particular, on average, the relative velocity vector $\mathbf{v}_{\mathrm{rel}}$, of the reactants and the laboratory velocity V_{CM}, of the centre of mass are coaxial with the guide. This

symmetry greatly simplifies the process of measuring product recoil velocity distributions. Gerlich [43] has developed a method based on TOF velocity measurements in variable rf trapping fields, that can measure the full two-dimensional differential cross-section. We have used this technique to probe the detailed dynamics of the reactions of $C_2H_2^+(v)+OCS$ and $OCS^+(v)+C_2H_2$ [12]; however, it is exceedingly tedious to use with our low-intensity low-repetition-rate state-selected ion beams. For the studies discussed below, we measured only the projections of the full velocity distributions on the octapole axis.

These 'axial velocity distributions' are substantially less time consuming to measure and analyse but, because of symmetry, retain the two most important pieces of dynamical information. When a complex forms in a collision, the orbital angular momentum of the collision partners goes into rotation of the complex. The rotational period τ_{rot} can be estimated from the *ab initio* structure of the complex, the collision energy and the average impact parameter leading to reaction (estimated from the magnitude of the cross-section). Typically, τ_{rot} ranges from 1 ps to a few picoseconds, depending on the reactant masses and collision energy. If reaction proceeds via a collision intermediate with lifetime long compared with its rotational period, the resulting axial velocity distributions must be forward–backward symmetric with respect to V_{CM} (forward is defined as faster than V_{CM}). Conversely, an asymmetric distribution implies a direct reaction where the collision time is short and also reveals the preferred direction of scattering (forward versus backward). The maximum deviation of the axial velocity distribution from V_{CM} is a measure of the maximum energy going into recoil of the products. To extract quantitative information from the product recoil velocity distributions, we fit them using the osculating complex model of Fisk *et al*. [44]. Fitting allows us to correct for experimental broadening factors (reactant velocity distributions) and to extract estimates for both collision time and the E_{recoil} distribution, [10, 12]. One caveat is that the apparent velocities of product ions with low laboratory energies are easily distorted by surface potentials on the octapole. For this reason, the reported distributions are truncated at velocities corresponding to about 100 meV laboratory energy.

In recent years we have begun to calculate the structures and energies of complexes and transition states using *ab initio* methods, implemented in the GAUSSIAN 98 package [45]. In addition, we have used the Rice–Ramsperger–Kassel–Marcus (RRKM) unimolecular rate program of Zhu and Hase [46] to calculate lifetimes and branching ratios for decomposition of intermediate complexes. This review presents some previously unreported *ab initio* results on the hydrogen-bonded complexes important in reaction of NH_3^+ with methanol.

3. $C_2H_2^+$ + methane

$C_2H_2^+$ + methane is an example of an unsaturated system, in which both electrostatic and covalently bound complexes are expected. Figure 3 shows a schematic reaction coordinate diagram. The energetics for the $C_3H_x^+$ products and covalently bound complexes are based on thermochemistry in the literature [47]. The non-covalent complexes, the transition state (TS) and the $C_2H_3^+$ product channels are taken from *ab initio* calculations by Klippenstein [48]. Note that there are two forms of $C_2H_3^+$. In the bridged form, the additional proton is symmetrically bound to the two carbon atoms. In the classical form the additional proton is bound to only one of the carbon atoms as $[CH_2CH]^+$. There are three non-covalently bound complexes, all of

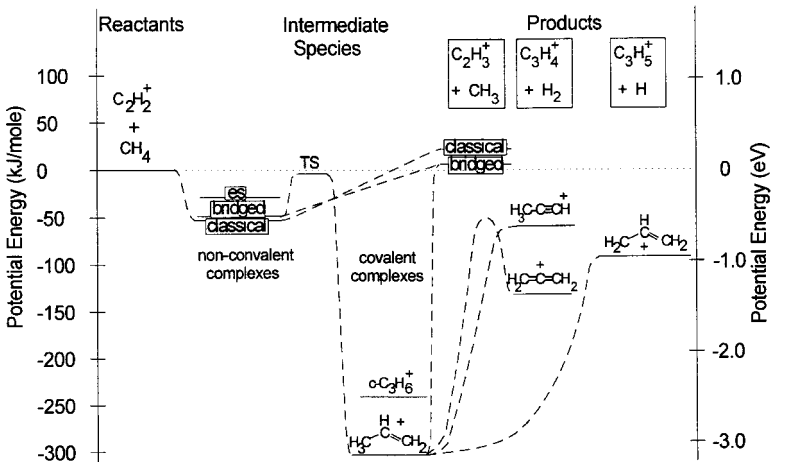

Figure 3. Reaction coordinate diagram for the reaction of $C_2H_2^+$ with CH_4. Both the non-covalently bonded (es, electrostatic) and covalently bonded intermediates play an important role in mediating reaction.

the form $C_2H_2^+$–CH_4, in which the intact reactant molecules are coordinated in different arrangements. In the experiments, we are not sensitive to such fine details of the complex or product structures. In the covalent complexes, the two most stable of which are indicated, C–C bonds are formed and hydrogen atoms are transferred in forming the complex.

The integral cross sections for the three major product channels are shown in figure 4 as a function of centre-of-mass collision energy, for three different vibrational states of the $C_2H_2^+$ reactant. The CC stretch is excited at v_2, with an energy of 1814 cm^{-1} (225 meV). The curve labelled 2 bend corresponds to ions with two quanta of the *cis* bend excited ($2v_5$ = 1253 cm^{-1} = 155 meV). The major reactions are

$$\begin{aligned} C_2H_2^+ + CH_4 &\rightarrow C_3H_5^+ + H, && \Delta E = -0.92 \text{ eV}, \\ &\rightarrow C_3H_4^+ + H_2, && \Delta E = -1.33 \text{ eV}, \\ &\rightarrow C_2H_3^+ + CH_3 \quad \text{(bridged)}, && \Delta E = +0.07 \text{ eV}, \\ &\rightarrow C_2H_3^+ + CH_3 \quad \text{(classical)}, && \Delta E = +0.23 \text{ eV}. \end{aligned}$$

The exoergic $C_3H_x^+$ channels require formation of C–C bonds and hydrogen atom migration along the carbon backbone. It seems reasonable, therefore, to propose that these products must form via H or H_2 elimination from the covalently bound complexes. We have examined isotope scrambling in reaction of $C_2H_2^+$ and CD_4 and, for these products, the distribution of isotopic products is approximately statistical for all collision energies studied, as might be expected for the covalent complexes. A striking feature of the $C_3H_x^+$ channels is how similar the collision energy and vibrational state dependences are for $C_3H_5^+$ and $C_3H_4^+$. Both reactions are inhibited by collision energy, slightly inhibited by CC stretch excitation and significantly enhanced by $2v_{bend}$ excitation. The similarities almost require that these two channels share a common critical point along the reaction coordinate, where the collision energy and vibrational dependence is determined. The fact that the vibrational effects are mode specific indicates that this critical point must be early in the reaction, before

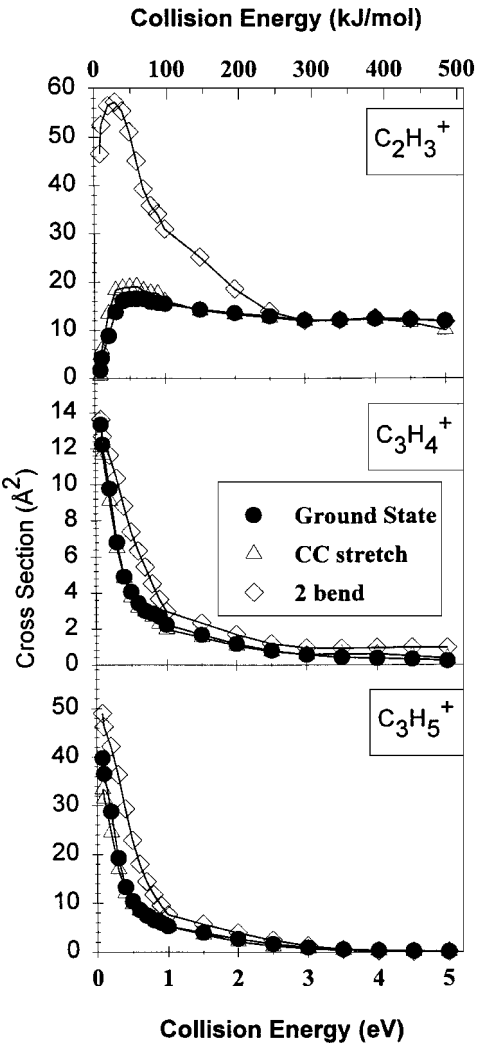

Figure 4. Cross sections as functions of collision energy for the indicated product of the $C_2H_2^+ + CH_4$ reaction. The different curves show the effect of excitation of different modes in the reactant ion. Note the dramatic effect of the bend.

the initial mode-specific vibrational excitation is scrambled. Such a critical point could occur as the reactants approach each other or, as Klippenstein [48] has suggested, at the TS (labelled in figure 3) separating the non-covalent and covalent complexes. The latter possibility requires that the vibrations have at least some chance of surviving for the lifetime of these non-covalent complexes.

Complete energy randomization is expected once the covalent complexes form, and it should be possible to treat their decomposition statistically. The estimated RRKM lifetime of the covalent complex (assuming the most stable form) varies from approximately 10 ns at our lowest collision energies to 70 ps at 3.0 eV. Because the barrier height for production of $C_3H_4^+ + H_2$ is not well known, it is not possible to model quantitatively the product branching out of the covalent complex. The trends with increasing energy are, however, correct. At low energies, the largest branching is

to $C_3H_5^+ + H$, which has the lowest activation energy. With increasing energy, the branching increases for the higher-energy products ($C_3H_4^+ + H_2$ and $C_2H_3^+ + CH_3$).

If this mechanism, dominated by statistical covalent complexes, is correct, we should expect to see forward–backward symmetric velocity distributions for the $C_3H_5^+$ and $C_3H_4^+$ product ions, with little energy going into recoil. Unfortunately, for these two product ions, the kinematics are very poor for measuring product velocities (little of the recoil velocity is partitioned to the heavy ion product that we are able to monitor). As we show below, however, the $C_2H_3^+$ velocity distributions are consistent with the covalent complexes behaving statistically. The only remaining question regarding this mechanism is the origin of the collision energy and vibrational effects (see below).

The $C_2H_3^+ + CH_3$ channel presents more interesting dynamical possibilities, as these products can form either by methyl elimination from the covalent complexes, or by direct hydrogen atom abstraction, possibly mediated by a non-covalent complex. In addition, the kinematics are more suitable for measuring product velocity distributions; so more detail is available. Finally, the large effect of *cis*-bending vibration is probably the most dramatic mode-specific vibrational effect ever recorded.

In the reaction of $C_2H_2^+$ with CD_4, approximately 10–15% of the '$C_2H_3^+$' product is $C_2HD_2^+$, that is, isotope scrambling occurs in a significant, but much smaller than statistical, fraction of collisions leading to hydrogen abstraction. This 'abstraction with exchange' channel is observed at all collision energies. Indeed, the $C_2HD_2^+$-to-$C_2H_2D^+$ ratio actually increases with increasing collision energy. Figure 5 shows a few selected axial recoil velocity distributions for hydrogen abstraction products at several collision energies. Figures 5(*a*)–(*c*) show recoil velocities at several collision energies for the reaction $C_2H_2^+ + CD_4 \rightarrow C_2H_2D^+ + CD_3$, that is abstraction without H–D exchange. Figure 5(*d*) shows the velocity of the $C_2HD_2^+$ product, that is H abstraction *with* H–D exchange. The heavy solid vertical line in each figure is the velocity V_{cm} of the centre of mass. As discussed above, for reactions that are mediated by a complex with lifetime greater than or equal to its rotational period, the axial velocity distribution must be forward–backward symmetric about V_{CM}. Within experimental error, the $C_2H_2D^+$ velocity distributions at collision energies below about 0.5 eV are forward–backward symmetric, but the distributions become progressively forward peaked at higher collision energies. Clearly, at high energies, the collision time is short compared with the rotational period (about 0.5 ps) and the gradual transition to forward–backward symmetry at lower energies suggests that the collision time increases to over a picosecond at low energies ($\tau_{rot} \approx 1.3$ ps at 0.4 eV). Osculating complex model fits to the velocity distributions reinforce this picture. At high collision energies, the fraction of the available energy $E_{avail} = E_{col} + E_{vib} + E_{rot} - E_{rxn}$ that appears as recoil energy is about 60%, decreasing to about 30% at low energies. Such a trend is consistent with the idea that, as the collision complex lifetime increases, there is increased opportunity for energy redistribution.

Figure 5(*d*) shows the velocity distribution at high collision energies for the product of hydrogen abstraction with H–D exchange (H–Dx). Note that this channel remains forward–backward symmetric, even at high collision energies. The conclusion is that the 'abstraction with exchange' channel requires a long-lived complex to allow time for the exchange. Given the well depths, this long-lived complex must be one of the covalent complexes, calculated to have a lifetime of about 70 ps at this energy. Further evidence that this channel involves a long-lived complex comes from the recoil energy distribution. Only about 10% of E_{avail} is found to appear in recoil energy

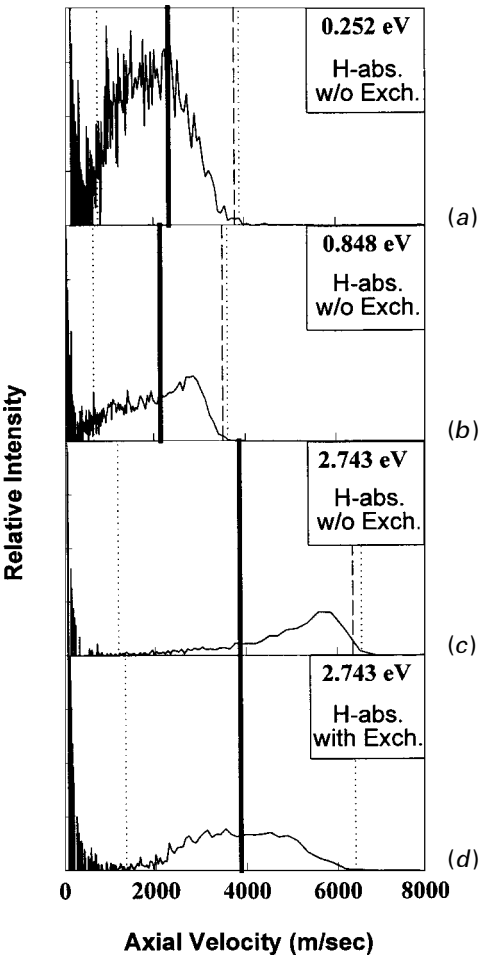

Figure 5. Product velocity distributions for the indicated product channels. The heavy vertical lines indicate the laboratory-frame velocity V_{CM} of the centre of mass. The broken vertical lines indicate the spectator-stripping limits. The dotted lines indicate the limit of velocities allowed by conservation of energy.

for abstraction with exchange, compared with 60% for abstraction without exchange.

The conclusion is that 15–23% (the percentage depending on collision energy) of the $C_2H_3^+ + CH_3$ products form by statistical decay of covalently bound $C_3H_6^+$ complexes (based on the isotopic combination statistics). The balance of $C_2H_3^+$ products form in collisions with time scales ranging from around 1 ps at low energies to less than 100 fs at high energies. To put these time scales in perspective, it is useful to estimate the 'direct' collision time, which we take, arbitrarily, as the time that it would take the reactants to fly past each other, if no momentum transfer occurred. Taking 5 Å as our reference distance scale, the direct collision time ranges from about 160 fs at 0.4 eV collision energy, to about 60 fs at 3 eV. At low collision energies, then, the observed collision time scale is five to ten times the direct collision time, indicating that the non-covalent complexes play a significant role in lengthening the time available for interaction between the reactants. At high energies, however, the

observed collision time scale is roughly equal to the direct time scale. Note that, in figures 5(*a*)–(*c*), there is a broken vertical line. This line indicates the laboratory velocity that the product ions would have if the mechanism was at the spectator-stripping limit, that is the limit of a direct stripping collision. By 2.74 eV collision energy, the peak of the experimental velocity distribution approaches the spectator-stripping limit, that is the direct collision limit.

The remaining dynamical issue is the origin of the vibrational effects. As already noted, the *cis*-bending vibration ($2\nu_5$ = 1253 cm^{-1}) results in significant enhancement of the $C_3H_x^+$ channels, and a very large enhancement of the hydrogen abstraction channel, particularly at low energies. In contrast, the CC stretch (ν_2 = 1814 cm^{-1}) has little effect on any of the reactions. For the endoergic hydrogen abstraction reaction, CC stretching has substantially less effect than adding the same amount of collision energy. There are several questions of interest as follows. At what point, or points, along the reaction coordinate does the bending vibration cause the enhancement? How does bending vibration affect reactivity and branching between the product channels? Does vibration influence product branching by controlling competition between the product channels, or by adding to overall reactivity?

The last question is the most easily answered; total reactivity substantially increases with bend excitation. The maximum enhancement is 270% at $E_{col} \approx 0.5$ eV, but there is a substantial enhancement at all energies below about 2 eV. In contrast, CC stretch excitation results in a 10% reduction in total cross-section for $E_{col} < 0.2$ eV and has no effect on either total or individual product cross-sections at higher energies. Note, however, that, while bending excitation enhances total reactivity, the enhancement is channel specific. For the $C_3H_x^+$ channels, the enhancement is a factor of at most about two while, for hydrogen abstraction, the enhancement can be a factor of up to 30 at low energies.

Bending may enhance reactivity at several points along the reaction coordinate. It might be that bending enhances the probability of trapping reactants into the weakly bound non-covalent complexes. Certainly the enhancement is largest in the low-collision-energy regime where the weakly bound complexes significantly increase the collision time scale (as shown by the recoil velocity distributions). Bending motion can be thought of as partially breaking the π bond in the bending plane; thus, one might expect bending to increase the tendency to form complexes. In particular, the $C_2H_2^+$ moiety in both the bridged and the electrostatic complexes (figure 3) is *cis* bent, and the electrostatic complexes are likely to mediate formation of the more strongly bound bridged and classical complexes. This is a 'dynamical' enhancement mechanism, in that bending is proposed to be a particularly favourable type of motion, that increases reactivity dramatically.

Klippenstein has proposed a 'statistical' mechanism, within the framework of TS theory. The proposal is that vibrational effects are the result of competition in break-up of the non-covalent complexes, and that the vibration simply provides available energy. The competition is between formation of covalent complexes that go on to $C_3H_x^+$ products, dissociation to $C_2H_3^+ + CH_3$ products, and break-up back to reactants. Obviously, a purely statistical model cannot account for highly mode-specific behaviour, as is observed here. Klippenstein has shown that the mode specificity can be qualitatively rationalized if a dynamical assumption is incorporated into the TS theory model. His proposal is that the CC stretching vibration is adiabatic in the non-covalent complexes, that is, so weakly coupled to other modes of the complex that its energy is not available to drive complex decay. The bending vibration,

on the other hand, is argued to be strongly coupled and thus contributes to the available energy in the complexes. As expected, the CC stretch, assumed to be uncoupled in the model, has little or no effect on reactivity or product branching, as is observed. Bending energy is correctly predicted to enhance the cross-section of the endoergic $C_2H_3^+ + CH_3$ reaction, although by a factor smaller than observed. Bending is also predicted to inhibit the $C_3H_x^+$ channels, whereas they are enhanced in the experiment. It appears that, even with the incorporation of the weak-coupling argument, a statistical picture cannot fully account for the observations. The implication is that there are dynamical consequences of specific vibrational excitations.

An important caveat in considering the role of covalently bound complexes is that the mere existence of deeply bound covalent complexes does not guarantee that such complexes are important in the reaction mechanism. For the reaction of acetylene with methane, these complexes are clearly important but, in several other systems with similar covalent complexes, we have found that the covalent complexes do not play a significant role at any collision energy, despite there being no barrier to accessing this region of the potential surface. For example, in the reaction of acetylene cation with methanol [20] and with ammonia [19], there are strongly bound $C_3H_6O^+$ and $C_2H_5N^+$ complexes that play no role in the reactions.

4. Phenol + ammonia

In the case of acetylene, it is not difficult to see that bending vibration can have a dynamical effect that increases the probability of complex formation owing to the distortion of the molecular orbitals in the acetylene cation. For phenol ammonia, the chemistry occurs in a hydrogen-bonded $C_6H_5OH^+$–NH_3 geometry; yet we observe substantial effects from excitation of low-frequency ring vibrations in $C_6H_5OH^+$ that involve no distortion of the hydroxyl moiety [16, 17].

Figure 6 shows a reaction coordinate energy diagram for the $C_6H_5OH^+ + ND_3$ system. The energetics are taken from our *ab initio* calculations [16], with the exception of the endoergicity for proton transfer, which was obtained from fits to our experimental cross-section (see below) [17]. The following reactions are observed:

$$\begin{aligned} C_6H_5OH^+ + ND_3 &\rightarrow C_6H_5OD^+ + ND_2H, && -0.007 \text{ eV}, \\ &\rightarrow C_6H_5O + ND_3H^+, && +0.195 \text{ eV}, \\ &\rightarrow [C_6H_5OH{:}ND_3]^+, && -1.2 \text{ to } -1.4 \text{ eV}, \\ &\rightarrow C_6H_5OH^+ + ND_3, && 0.00 \text{ eV}. \end{aligned}$$

The first channel is H/D exchange (H–Dx); the exothermicity of this channel originates from the zero-point energy differences of the products and reactants. The second channel is proton transfer (PT), which we find to be endoergic. The third channel corresponds to formation of a metastable collision complex, some small fraction of which survives long enough to be detected. The final channel corresponds to no reaction, but we include it in the list to emphasize that this is one of the channels for decomposition of any intermediate complexes that form in the collisions.

The energetics for the complexes and TSs shown are from second-order Møller–Plesset (MP2)/6-31G* calculations. We have also calculated the complex energies at the quadratic configuration interaction singles plus doubles with

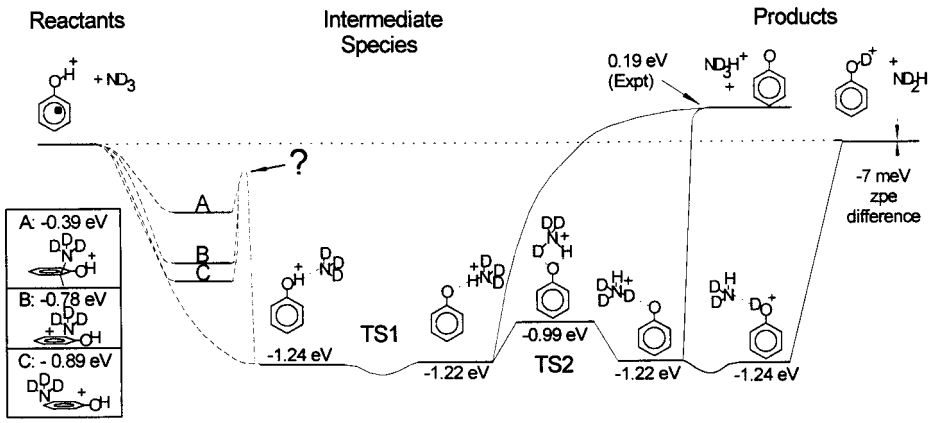

Figure 6. Reaction coordinate diagram for the reaction of $PhOH^+ + ND_3$. See text for details about the energies. TS1 is a barrier on the electronic energy surface, but there is no barrier when zero-point energy (zpe) is included.

perturbative triples (QCISD(T))/6-31G(d) level of theory, and find binding energies that are 0.1–0.2 eV greater. The MP2 results are shown here because QCISD(T) results are not available for the TSs. Yi and Scheiner [49] also reported *ab initio* calculations on the hydrogen-bonded complexes, which are generally in accord with ours.

The important points are as follows.

(i) There are hydrogen-bonded complexes, as expected, with binding energies greater than 1.2 eV.
(ii) There is no significant barrier to intracomplex proton transfer (i.e. interconversion between $C_6H_5OH^+$–ND_3 and C_6H_5O–HND_3^+).
(iii) The barrier to H–Dx exchange (TS2 in figure 6) is small compared with the binding energy of the complexes.
(iv) There are several non-hydrogen-bonded adducts that we term 'ND_3-on-ring' complexes. Two of these (B and C) are coordination-type complexes. Complex A is covalently bound, but with such a weak binding energy that it probably is not important in the reaction mechanism.
(v) We were not able to calculate the TS(s) separating the 'ND_3-on-ring' complexes and the hydrogen-bonded complexes, but a series of single-point calculations suggests that there is a substantial barrier.

Integral cross-sections for reaction with the ground-state phenol cation are shown in figure 7(*d*) for each of the three channels. Also shown, as a solid line is the collision cross-section, estimated as the ion–dipole capture cross-section [50] or the hard-sphere cross-section, whichever is greater. The ratio of a reaction cross-section to the collision cross-section is a measure of the reaction efficiency. The efficiency of H–Dx is approximately 40% at low collision energies, dropping to only a few per cent for collision energies above 1 eV. For PT, the efficiency is never more than a few per cent, because the endoergic PT reaction is not efficient at competing with the other channels. Similarly, adduct formation (AF) is never a very efficient process. By measuring the velocity distribution of the $C_6H_5OH^+$ carefully, it is possible to determine the fraction of parent ions that have suffered a highly inelastic but non-reactive collision. These ions correspond mostly to collisions where a complex formed and then decomposed

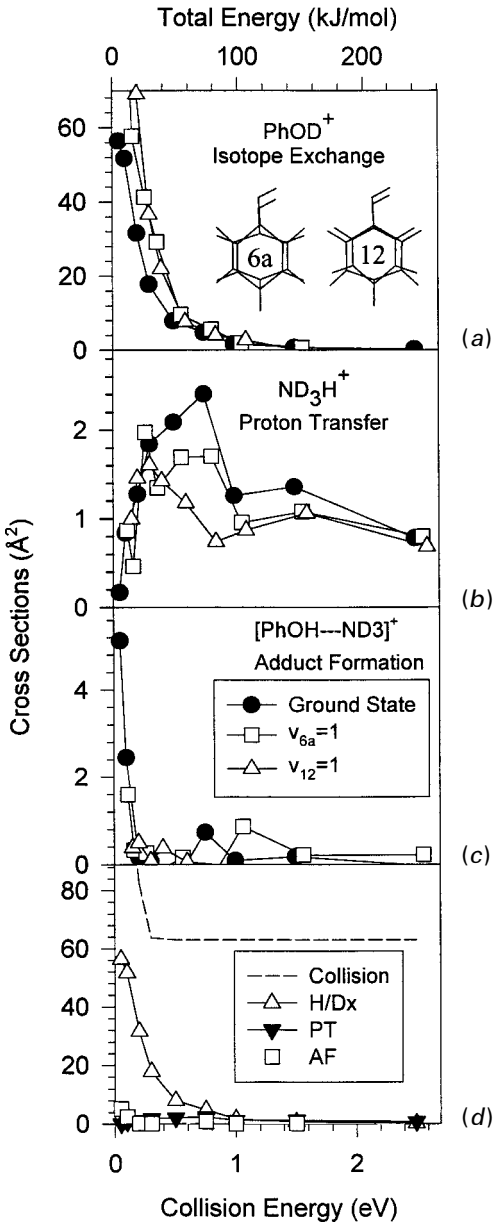

Figure 7. (*a*)–(*c*) cross-sections as functions of total (collision+vibrational) energy for the product channels of the $PhOH^+ + ND_3$ reaction. Note the different scales. (*d*) Cross-sections for the reaction of the ground-state ion as functions of collision energy. Also shown is an estimate of the collision cross-section.

back to reactants (i.e. the final product channel listed above). We can estimate that these deep inelastic non-reactive scattering events occur in about 20% of collisions at low energies, increasing to about 40% at high energies.

In addition to the ground state, we studied the reaction with excitation in two x-sensitive ring vibrations, $v_{6a} = 1$ and $v_{12} = 1$ (illustrated in the inset of figure 7(*a*)). Figures 7(*a*)–(*c*) compare the cross-sections for reaction of ground-state and

vibrationally excited $C_6H_5OH^+$, plotted as a function of the total, that is vibrational + collisional, energy.

AF is a minor channel but, because of its mechanistic import, we discuss it first. The observed cross-section for this channel is really a cross-section for formation of the adduct convoluted with the probability that the adduct survives to be detected. Such adducts are usually too short lived to be observed, the exception being reactions, such as this reaction, where there are strongly bound complexes, combined with the absence of reaction channels having substantial exoergicity. To have any chance of being detected in our experiment, the lifetime of the adduct must be at least in the tens of microseconds range. As expected, adducts are detected only at the lowest collision energies. RRKM calculations on the two hydrogen-bonded complexes give a lifetime of about 18 μs at our lowest collision energy, 0.05 eV. More importantly, the RRKM calculations indicate that the complexes A–C in figure 6 are not nearly stable enough to support such long lifetimes. In reaction with phenol-d_5 ($C_6D_5OH^+$) the adduct detection cross-section increases by a factor of four, consistent with the RRKM prediction of a sixfold to eightfold increase in lifetime caused by the decreasing ring vibrational frequencies. Within our signal-to-noise ratio the effect of vibrational energy on AF and survival is roughly equivalent to the effect of collision energy.

At low collision energies, the dominant channel is H–Dx. The mere observation of the H–Dx channel is suggestive of a reaction mediated by a long-lived complex, as isotope exchange requires an interaction that survives long enough to transfer at least two atoms. Product recoil velocity distributions are forward–backward symmetric at all energies, consistent with such a mechanism. Fits with the osculating complex model suggest that only a small fraction of the available energy goes into product recoil, also consistent with reaction through a long-lived complex. Figure 6 indicates the lowest-energy reaction pathway for H–Dx. First note that, in the $[C_6H_5OHND_3]^+$ hydrogen-bonded complex, there is no significant barrier to intracomplex proton transfer ($C_6H_5OH^+$–$ND_3 \leftrightarrow C_6H_5O$–$HND_3^+$); thus these two forms of the complex are expected to interconvert rapidly compared with the lifetime of the complex. The only significant barrier along the H–Dx reaction coordinate is TS2, which is still far less than the available energy in the complex. RRKM modelling indicates that H–D scrambling should be complete at low collision energies. Only at energies above about 1.5 eV should the lifetime of the hydrogen-bonded complex become short enough to prevent complete scrambling.

At low energy, H–Dx occurs in about 40% of collisions, dropping rapidly with increasing energy. Experiments with a deuterium-labelled phenol cation show that only the hydroxyl hydrogen can exchange with the ammonia deuterium atoms. Based on the number of exchanging hydrogen and deuterium atoms, one might expect that about 75% collisions leading to hydrogen-bonded complex formation ought to result in isotope exchange. In fact, the H–Dx probability is around 80%, because of the 7 meV exothermicity owing to zero-point effects. The efficiency observed at low energy is about half this expectation, indicating that hydrogen-bonded complexes form in only about half the collisions at low energies. Furthermore, the declining H–Dx efficiency implies that hydrogen-bonded complex formation declines rapidly with increasing collision energy.

Inefficient formation of hydrogen-bonded complexes is unsurprising on geometric grounds. The hydroxyl group is a relatively small target, and most collisions are expected to be in 'ND_3-on-phenyl-ring' geometries. One might expect that long-range forces could orient the reactants and increase the fraction of 'ND_3-on-hydroxyl'

collisions. In fact, the centre of charge of the phenol cation is close to the centre of the phenyl ring (small full circle superimposed on the phenol cation reactant structure in figure 6), thus the dominant long range force will tend to favour ND_3 on ring collision geometries.

There are two surprising observations, however. In the reaction with $C_6D_5OH^+$, the H–Dx efficiency at low energies is roughly doubled. This effect cannot be explained by the longer lifetime of the deuterated hydrogen-bonded complex, because the lifetime is already far longer than required for H–D scrambling. The implication is that ring deuteration somehow substantially enhances the probability of accessing the hydrogen-bonded geometry where H–Dx can occur. Similarly, excitation of either $C_6H_5OH^+$ vibrational mode leads to a substantial increase in the H–D efficiency, opposite to the effect of increasing collision energy. Again, the implication is that these in-plane ring vibrations must, somehow, increase the probability of accessing the hydrogen-bonded complexes.

Our explanation for both the deuteration and the vibrational effects invokes involvement of a precursor complex in the mechanism. As already noted, 'ND_3-on-ring' collisions are relatively likely, and as figure 6 shows, there are ND_3-on-ring complexes with binding energies approaching an electronvolt. At low collision energies, it seems likely that a large fraction of collisions will initially form 'ND_3-on-ring' complexes. The H–Dx probability is, in that case, strongly dependent on the probability that these ring-bound complexes can isomerize to the hydrogen-bound geometry, before complexes dissociate back to reactants. At low collision energies, both the formation of the ring-bound complexes and the isomerization step are reasonably efficient, leading to the observed 50% probability for forming the hydrogen-bonded complexes. The rapid decrease in reaction efficiency with increasing collision energy can then be understood in terms of decreased probability for trapping into the weak ring-bound wells, combined with decreasing probability for isomerization to the hydrogen-bonded complexes. Such a mechanism can also explain the effect of deuteration on the H–Dx efficiency. Deuteration of the ring increases the density of states of the precursor complex, increasing the complex formation probability and also increasing the lifetime of the complex by a factor of ~ 3.6. Because the TS to isomerization is lower in energy than the centrifugal barrier to dissociation back to reactants, deuteration will also favour isomerization over dissociation. The increase in efficiency with vibrational excitation is difficult to explain in a purely statistical picture and rather indicates a dynamical effect, that is, that vibrational excitation promotes the ring to hydrogen-bonded isomerization.

The PT channel displays a threshold to reaction at a low energy and in addition is inefficient compared with isotope exchange. This behaviour suggests either an energy barrier or a bottleneck to reaction. As noted above, any barrier to PT within the hydrogen-bonded complex is negligible. The fact that isotope exchange is relatively efficient is also evidence against a substantial barrier or kinetic bottleneck to PT within the hydrogen-bonded complex. A barrier in the exit channel of the hydrogen-bound complex above the dissociation energy would be unexpected for an ion-radical pair. We tested this possibility by performing MP2/6-31G* calculations mapping out the separation coordinate and found that the energy varied smoothly towards the dissociation limit. The conclusion is that PT is endoergic.

To estimate the endoergicity, we performed Monte Carlo simulations of the threshold as described above, in which the endoergicity was an adjustable parameter. We performed the simulation in two ways: a line-of-centres model fit to the energy

dependence of the PT cross-section, and a RRKM-based simulation of the experimental PT branching ratio. The first approach is appropriate in the limit of a direct reaction; the second assumes statistical decay of a long-lived complex. The endoergicities extracted with the two approaches were almost identical: 200 ± 40 meV for the line-of-centres model, and 195 ± 40 meV for the statistical model. If we correct the 195 eV value for the all-H-isotope combination and convert to a 298 K value, we obtain 204 ± 40 meV (4.7 ± 1 kcal mol^{-1}).

This value can be compared with previous literature values as follows. The endothermicity is the difference in proton affinities (PAs) of ammonia versus phenoxy. The PA of ammonia, 204.0 kcal mol^{-1} [51] is usually taken as a standard. Using this value and our value of the endothermicity of the PT reaction, we predict a PA for the phenoxy radical of 208.7 kcal mol^{-1}. This value may be compared with previous literature values of 204 kcal mol^{-1} [51] and a more recent value of 205 kcal mol^{-1} [52]. Note, however, that our result is consistent with the OH bond energy for neutral phenol recently reported by DeTuri and Ervin [53].

Two pieces of evidence indicate that the PT channel is mostly the result of a direct reaction; the product recoil velocity distributions are asymmetric, and the branching ratio for this channel from RRKM calculations is substantially smaller than the experimental branching (although with the same energy dependence). It appears that only a small fraction (about 10%) of the PT channel results from statistical decay of a long-lived complex.

The 'big picture' for this system is that reaction is mediated by several different complexes. At low collision energies, most collisions initially form precursor complexes, some of which isomerize into the more stable hydrogen-bonded complex, where H–Dx and PT reactions can occur. The efficiency of the H–Dx channel in particular is probably controlled to a large extent by the isomerization efficiency. The effects of both collision energy and ring deuteration can be readily understood in terms of the precursor complex model. To explain the effects of vibration appears to require that some dynamics be invoked, that is vibrational energy is somehow different from collision energy. We have proposed that the vibrational effect is manifest in the isomerization from ring-bound to hydrogen-bonded complexes. In order for this to be possible, it is necessary that the reactant vibration be preserved during the lifetime of the precursor, so that the energy is still in vibration at the time of isomerization. Our *ab initio* results are consistent with this picture, that is the ν_{6a} and ν_{12} vibrational frequencies remain very similar in the precursor complexes to their values in the free phenol cation, and the modes in the complex show little coupling of ND_3 motion to the vibration of the ring. In such a case, it is not unreasonable that a vibration might remain uncoupled to other modes of the complex for tens or hundreds of picoseconds. On the other hand, if the vibration is to have an effect on the isomerization process, vibration must couple to the reaction coordinate at that point. Again, the *ab initio* results are consistent with this picture. It appears that the potential for motion of the ND_3 relative to phenol cation is relatively flat for motion over the phenyl ring, but there is a large barrier associated with ND_3 passing the hydroxyl oxygen atom. At this point, that is at the isomerization barrier, the phenol vibrations, both of which involve considerable motion of the hydroxyl oxygen atom, will couple strongly to the ammonia moiety.

5. Ammonia + methanol

In the case of $C_6H_5OH^+ + ND_3$, the two forms of hydrogen-bonded complex ($C_6H_5OH^+$–ND_3 and C_6H_5O–HND_3^+) are not separated by a significant barrier and

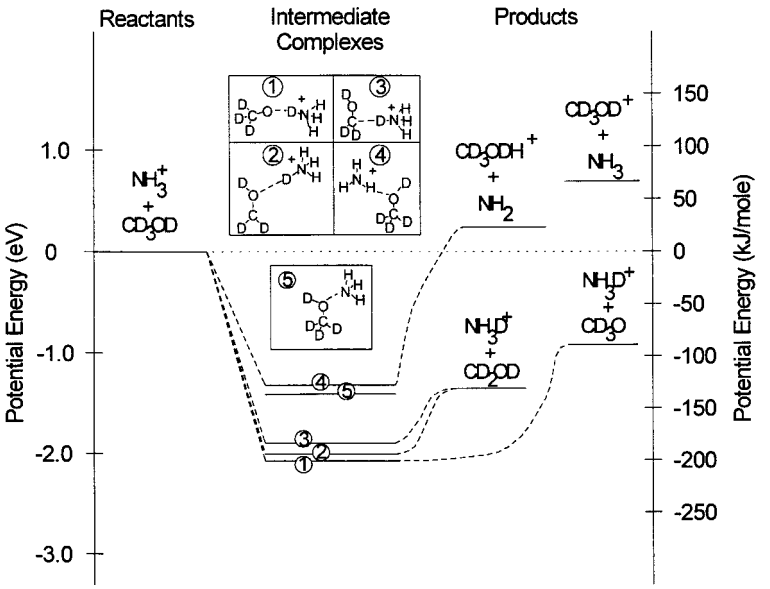

Figure 8. Reaction coordinate diagram for the reaction of NH_3^+ with CD_3OD. *Ab initio* complex geometries and energies were calculated for this review.

effectively form a single potential well. The reaction of ammonia cation with methanol, in contrast, is a case where formation of different hydrogen-bonded complexes results in different product channels. As a consequence, it appears that the outcome of the reaction is largely determined by competition in formation of different hydrogen-bonded complexes.

The reaction of the ammonia cation with CD_3OD has the following channels:

$$\begin{aligned} NH_3^+ + CD_3OD \rightarrow\ & NH_3D^+ + CD_3O, && \Delta E = -1.33\ \text{eV},\\ & NH_2D_2^+ + CD_2HO, && \Delta E = -0.9\ \text{eV}\\ & NH_2D_2^+ + CD_2OH && \\ & \text{(or CHDOD)}, && \Delta E = -1.33\ \text{eV},\\ & CD_3OD^+ + NH_3 && \Delta E = +0.69\ \text{eV},\\ & CD_3OHD^+ + NH_2, && \Delta E = +0.25\ \text{eV}. \end{aligned}$$

The energies given are taken from Lias *et al.* [47] and do not include zero-point differences in isotopomers. In our original study of this system [14], we speculated about the existence of three different hydrogen-bonded complexes. For the present paper, we have used *ab initio* calculations to search for intermediate complexes, and figure 8 shows the resulting reaction coordinate diagram. Five intermediate complexes were located at the B3LYP/6-31G* level of theory. Complexes 1–4 are hydrogen bonded, and complex 5 has the oxygen lone pair on methanol, coordinated to the positively charged nitrogen atom in NH_3^+. Complex 1 is the most stable with a binding energy of 2.05 eV relative to reactants and can be described as a hydrogen-bonded complex where the bond is between a hydrogen (deuterium) on an ammonium moiety with oxygen on a methoxy moiety. This complex was located in an optimization started in CD_3OD–NH_3 geometry, indicating that intracomplex abstraction of the hydroxyl hydrogen atom is exoergic with no barrier. Complex 2 is nearly isoenergetic

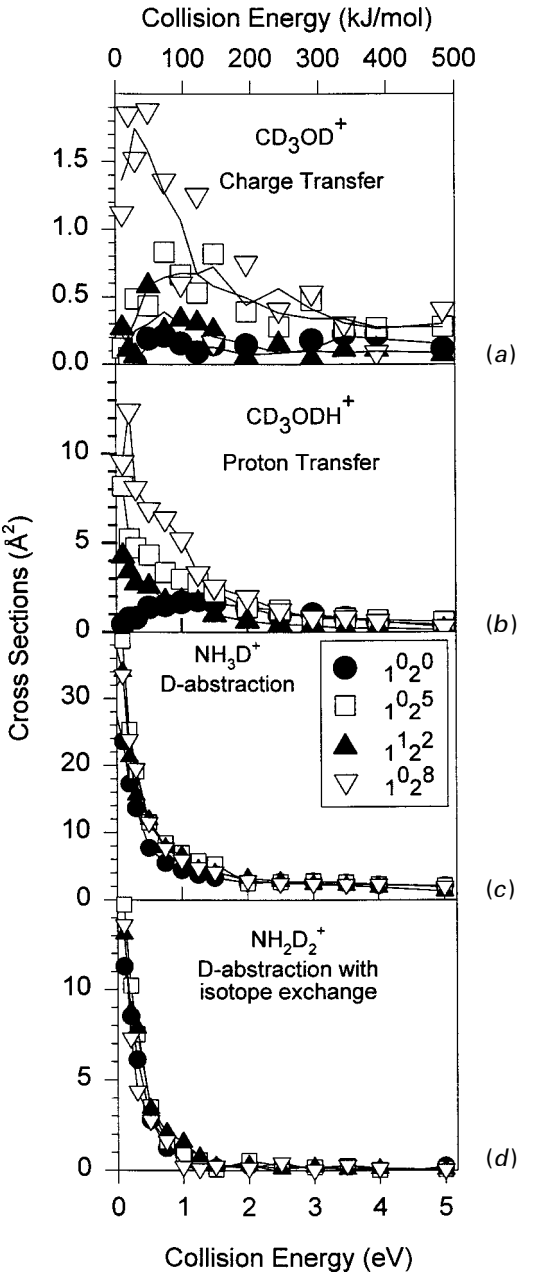

Figure 9. Cross-sections for each product channel as functions of collision energy and NH_3^+ reactant ion vibrational state.

with complex 1 at an energy of −2.04 eV. This complex was located in an optimization started in a geometry with the methanol hydrogen bonded through a methyl C–D bond to ammonia ($DOCD_3$–NH_3), indicating that intracomplex abstraction of a methyl hydrogen atom is also barrierless, as is the migration of the resulting ammonium cation to the oxygen centre. Complex 3 is bound by 1.90 eV. As in complex 2, the ammonia has abstracted a methyl hydrogen, but the resulting ammonium cation

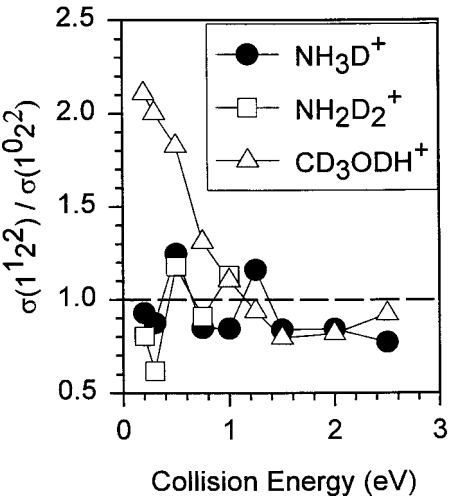

Figure 10. Ratio of the cross-sections for NH_3^+ with 1^12^2 excitation to those for 1^02^2 excitation for the three major channels of the $NH_3^+ + CD_3OD$ reaction. Although the ν_1 mode cannot be excited individually, its effect can be seen from this ratio.

has not migrated to the oxygen centre. The difference between complexes 2 and 3 is that the optimization of complex 2 was started with NH_3 attacking the methyl deuterium atom that is *trans* to the hydroxyl group (i.e. 180° DCOD dihedral angle), while complex 3 was started attacking one of the methyl deuterium atoms most hindered by the hydroxyl group. Evidently there is a small barrier to rotation around the C–O bond, preventing complex 3 from isomerizing to complex 2. In the real complex, there is substantial available energy, and this isomerization is probably facile. Complexes 4 and 5 involve bonding of an ammonia ion moiety with a methanol moiety. Complex 4 at −1.36 eV involves a hydrogen bond between a hydrogen atom on ammonia with the oxygen atom. The more stable complex 5 at −1.42 eV is a coordination-type complex with interaction between the oxygen lone pair and the half-filled nitrogen orbital.

Note that the first two product channels, deuterium abstraction (DA) from hydroxyl, and DA from methyl, are indistinguishable by mass without a mixed-isotope study. Previous thermal studies were made without vibrational state selection or isotopic substitution, reporting rates for NH_4^+ production that were between approximately 40 and 100% of the collision rate [54–56]. NH_4^+ was the only channel found in these studies, which is not surprising as the charge-transfer (CT) and PT channels are endothermic, and isotopic substitution is necessary to distinguish the exothermic channels producing NH_4^+.

In our study [14] we examined the reaction of NH_3^+ with CD_3OH and CH_3OD as well as CD_3OD. Except where otherwise specified, we refer to the reaction of NH_3^+ with CD_3OD. We studied this reaction with the NH_3^+ reactant in five different vibrational states: 1^02^0, 1^02^2, 1^02^5, 1^02^8, 1^12^2, where the number of quanta of excitation of the ν_1 (symmetric stretch) and ν_2 (umbrella bend) are shown as superscripts.

Figure 9 shows cross-sections for the four distinguishable channels as functions of collision energy. Note the different scales for figures 9(*a*), (*b*), (*c*) and (*d*). We label the distinguishable channels as follows. Production of CD_3OD is CT; production of CD_3ODH^+ is PT; production of NH_3D^+ is DA; production of $NH_2D_2^+$ is deuterium abstraction with isotope exchange (DAX). Figure 10 shows the ratio of cross-sections

for excitation of the $1^1 2^2$ and $1^0 2^2$ excitations to separate out the effects of v_1, which we can only populate via the combination band. The cross-section for CT is too small to allow calculation of a meaningful ratio, as is the cross-section for DAX above 1 eV.

Production of NH_3D^+ results from DA either from the methyl group or the hydroxy group of methanol-d_4. A low E_{col}, this channel is suppressed by collision energy and enhanced by the v_2 umbrella bend with the largest enhancement for five quanta of bend. The symmetric stretch has no effect within our uncertainties when the effect of the bend is removed from the combination band (figure 10). Above $E_{col} \approx$ 2 eV, the cross-section is insensitive to collision energy or vibrational excitation.

To address the question of whether the deuterium is abstracted from the methyl or hydroxy moieties, we conducted experiments with CD_3OH and CH_3OD. Note that abstraction from methyl is energetically more favourable than from hydroxy. One would expect therefore that methyl DA should dominate at low energies, both because of the relative energetics and because there is a 3:1 ratio of methyl:hydroxyl abstraction sites. One of the more interesting observations is that, contrary to expectation, the methyl:hydroxyl DA ratio is about unity. Furthermore, at high collision energies, where the difference in ΔH_{rxn} is insignificant, we might expect that the ratio should become statistical (3:1). Again, counter to expectation, the ratio at higher energies deviates further and further from the statistical value. Abstraction from methyl is dominant by a factor of about five by 2 eV and a factor of 40 by 3 eV. We found no significant effect of vibration on the branching between these two channels.

Recoil velocity distributions were measured for the reactions of both CD_3OH and CH_3OD. For both channels at E_{col} = 2.5 eV the NH_3D^+ is forward scattered with the peak of the distribution near the spectator-stripping limit, that is a large fraction of the collision energy goes into recoil. At lower $E_{col} \approx 1$ eV, abstraction from hydroxy gives a narrow velocity peak centred about V_{CM}, suggesting that abstraction from hydroxyl proceeds via a long-lived (greater than 500 fs) complex at this energy. For abstraction from methyl at 1 eV, the distribution appears forward peaked, with considerably more energy appearing in recoil than for abstraction from hydroxyl. The implication is abstraction from the methyl group is still predominantly a direct reaction 1 eV collision energy. At $E_{col} \approx 0.37$ eV, abstraction from both hydroxyl and methyl groups leads to distributions that are forward–backward symmetric, with little energy appearing in recoil, consistent with reaction through a long-lived (greater than 1 ps) complex.

At low collision energies, where complex-mediated reactions are important, we propose that the branching between DA from methyl and hydroxy sites depends on the nature of the complex formed. For example, one would expect complex 1 to lead to abstraction from hydroxy, whereas complexes 2 and 3 should lead to abstraction from methyl. The fact that the more stable complex 1 leads to the less stable products ($CD_3O + NH_3D^+$) presumably explains the larger-than-expected branching to this channel; product branching is controlled by complex formation and not product energetics. The enhancement of both hydroxyl and methyl DA reactions by the umbrella bend (v_2), can be explained by the fact that this motion distorts the ammonia cation away from its planar geometry, making the formation of complexes 1, 2 and 3, in which ammonia assumes a pyramidal geometry, more facile. The ratio of abstraction from the hydroxy group to that from the methyl group is not affected by this vibration, indicating that this motion does not change the relative probability of forming complexes 2 and 3 versus complex 1 but rather increases the probability of forming these

three complexes relative to complex 4. At $E_{col} \approx 1$ eV, abstraction from methyl, the more exothermic abstraction channel, has an important contribution from a direct reaction, while abstraction from the methyl group occurs by a complex-mediated mechanism. The observation that the two channels are dynamically distinct, tends to support the notion that the complex 1 does not interconvert with complexes 2 and 3 on the collision time scale.

We now consider the DAX channel. This channel is expected to require a long-lived complex intermediate, because three atoms are transferred: two deuterium atoms from ammonia to methanol and one hydrogen atom from methanol to ammonia. It is, therefore, not surprising that the DAX reaction is only significant at low collision energies, where complex lifetimes are long. One question is whether the DAX reaction involves atom exchanges at both oxygen and carbon centres in the methanol reactant, or whether only methyl deuterium atoms are exchanges. This question was addressed by examining DAX in reaction of NH_3^+ with CD_3OH. Somewhat surprisingly, no $ND_2H_2^+$ was observed, indicating that there must be deuterium present in both the methyl and the hydroxy groups. As already noted, it is likely that interconversion is facile between complexes 2 and 3, that is the ammonium cation can hydrogen-bond to both the oxygen and the carbon centres in CD_2OD. DAX most probably occurs in a sequential manner, and there may be more than one sequence leading to the DAX products. For example, NH_3^+ might abstract deuterium from the methyl group; the NH_3D^+ moiety might then isomerize to complex 3. Rotation of the NH_3D^+ moiety sets the system up to transfer H^+ to the hydroxyl oxygen atom, followed by abstraction of another deuterium atom to form the $ND_2H_2^+$ product. We have not attempted to calculate the barriers to isomerization or ammonium rotation, but we note that ammonium rotation in NH_4^+–phenoxy complexes has a barrier of only about 0.3 eV. If the barriers in this system are comparable, the isomerization process should be fast compared with the lifetimes of the complexes, that is DAX should be relatively efficient at low collision energies. As the collision energy increases, the complex lifetimes drop rapidly, thus shutting down the DAX reaction, as observed. Certainly, the recoil velocity distributions are consistent with a mechanism at low energies mediated by a long-lived complex. The distributions are forward–backward symmetric, and only 4–5% of the available energy appears as product recoil. At all collision energies, the recoil energy for the DAX products is substantially lower than for the DA products, indicating that the complex lifetime required to mediate DAX is longer than for DA.

Figure 9(*a*) shows the cross-sections for the endoergic CT channel. Note that for the ground state there is negligible cross-section for this channel even at high collision energies. This observation shows that collision energy is not effectively converted to the electronic energy necessary to drive CT. The ν_2 umbrella bend, in contrast, is effective at driving this reaction. For example, the $1^0 2^5$ reactant state has about 0.60 eV of ν_2 vibrational energy, nearly enough to overcome the CT endoergicity. In the $1^0 2^8$ state, the umbrella bending energy is, by itself, sufficient to drive CT. For this state, there is a substantial increase in CT cross-section, although the efficiency is still only about 1%. Comparison of the $1^1 2^2$ and $1^0 2^5$ states, which have similar vibrational energies, distributed differently, indicates that the symmetric stretch ν_1 has a negligible effect on CT.

For the $1^0 2^8$ state, the signal is large enough that we can measure recoil velocity distributions. At low collision energies, the distributions are consistent with forward–backward symmetric scattering while, at $E_{col} \approx 1$ eV, the distribution is somewhat

backward peaked. This result suggests that, at high energies, CT can proceed in short direct collisions while, at low energies, a more intimate collision is required. In this case, CT is in competition with the more energetically favourable DA and DAX reactions.

The PT channel is also endoergic. For the ground state, the threshold behaviour at low collision energies shows that the collision energy is efficient in overcoming the PT endoergicity, in contrast with CT where the collision energy is ineffective. All vibrations also enhance the reaction to a greater extent than the collision energy does. For a collision energy just above threshold (about 0.25 eV), adding 0.6 eV of vibrational energy ($1^0 2^5$) results in a nearly sixfold enhancement, in contrast with the twofold effect of adding an equivalent amount of collision energy. For the umbrella bend the enhancement is roughly proportional to the vibrational energy. The symmetric stretch enhances the reaction as well but not as effectively as the umbrella bend (figure 10). This channel is the only one in which the stretch is observed to promote reaction.

At low collision energies, the PT recoil-velocity distributions are symmetric and narrow, that is, consistent with a complex-mediated mechanism. The fact that both umbrella bend and symmetric stretch vibrations enhance reaction, in contrast with the other channels where only the umbrella bend is active, suggests that the complex involved is different from those mediating the other channels. We have proposed that the PT reaction is mediated by the H_2NH–$ODCD_3$ complex (complex 4), and that the relatively low stability of this complex is at least partly responsible for the low PT efficiency. At high energies, this channel gives a velocity distribution that clearly indicates a direct reaction, near the stripping limit. Even at high energies, the efficiency is quite low, only 2–3% of the hard-sphere cross-section. Vibration has no effect at these energies and the effect of the collision energy is small. Presumably, the reaction probability at high collision energies is dominated by the impact geometry.

The reaction of ammonia cation with methanol is an example where the nature of the intermediate complexes formed has a direct effect on the outcome of the reaction. The implication from our results is that the branching between formation of different complexes is dominant in determining the outcome of the reaction at low collision energies. In other words, the most significant dynamical behaviour is competition between the entrance channels to complexes 1, 2 and 3, rather than in the method that a complex decays.

6. Conclusion

We have presented three different studies of ion–molecule reactions for which the results suggest that significant features of the reaction mechanism are best explained by the behaviour of intermediate complexes. In the first example, reaction of acetylene cation with methane, mode-specific effects are manifest primarily at the TSs leading from the weakly bound short-lived complexes to the covalently bound complex or to the hydrogen abstraction product. In the second case, the reaction of phenol cation with ammonia, precursor complexes again mediate transition to the more strongly bound complex where reaction occurs. In this case, the strongly bound complex is hydrogen bonded. Vibration appears to be effective in driving isomerization to the hydrogen-bonded geometry, whereas the collision energy shortens the precursor lifetime and drastically reduces the reaction efficiency. In the reaction of ammonia cation with methanol, it is formation of long-lived hydrogen-bonded complexes that determines the ultimate product channel. In this reaction, even at low collision energies, the choice between product channels is made early in the collision, and the

main effect of vibration is on the formation probability of the hydrogen-bonded complexes. Weakly bound electrostatic complexes are not thought to be important in the reaction mechanism.

Acknowledgements

The research was funded by the National Science Foundation under grant CHE-9807625. We are also grateful for support from the Utah Center for High Performance Computing. The SGI Origin 2000 used for some of the calculations was partly funded by the SGI Supercomputing Visualization Center Grant.

References

[1] Bowers, M. T., 1979, *Gas Phase Ion Chemistry* (New York: Academic Press).
[2] Ng, C. Y., 1992, *Adv. chem. Phys.*, **82**, 401.
[3] Ng, C. Y., and Baer, M. (editors), 1992, *State-selected and State-to-state Ion–Molecule Reaction Dynamics*, Part 1, *Experiment*, Part 2, *Theory* (New York: Wiley–Interscience).
[4] Alge, E., Villinger, H., Pesca, K., Ramler, H., and Lindinger, W., 1979, *J. Phys., Paris*, C7–83.
[5] Anderson, S. L., 1991, *NATO Adv. Study Inst. Ser., Ser.* C, **347**, 183.
[6] Anderson, S. L., 1992, *Adv. chem. Phys.*, **82**, 177.
[7] Anderson, S. L., 1997, *Accts chem. Res.*, **30**, 28.
[8] Chiu, Y.-H., Yang, B., Fu, H., Anderson, S. L., Schweizer, M., and Gerlich, D., 1992, *J. chem. Phys.*, **96**, 5781.
[9] Chiu, Y.-H., Fu, H., Huang, J.-T., and Anderson, S. L., 1994, *J. chem. Phys.*, **101**, 5410.
[10] Chiu, Y.-H., Fu, H., Huang, J.-T., and Anderson, S. L., 1995, *J. chem. Phys.*, **102**, 1199.
[11] Chiu, Y.-H., Fu, H., Huang, J.-T., and Anderson, S. L., 1995, *J. chem. Phys.*, **102**, 1188.
[12] Chiu, Y.-H., Fu, H., Huang, J.-T., and Anderson, S. L., 1996, *J. chem. Phys.*, **105**, 3089.
[13] Fu, H., 1997, PhD Thesis, State University of New York.
[14] Fu, H., Qian, J., Green, R. J., and Anderson, S. L., 1998, *J. chem. Phys.*, **108**, 2395.
[15] Green, R. J., Kim, H.-T., Qian, J., and Anderson, S. L., 2000, *J. chem. Phys.*, **113**, 3002.
[16] Green, R. J., Kim, H.-T., Qian, J., and Anderson, S. L., 2000 *J. chem. Phys.*, **113**, 4158.
[17] Kim, H.-T., Green, J. J., Qian, J. and Anderson, S. L., 2000, *J. chem. Phys.*, **112**, 5717.
[18] Kim, H.-T., Green, R. J., and Anderson, S. L., 2000, *J. chem. Phys.*, **113**, 11079.
[19] Qian, J., Fu, H. and Anderson, S. L., 1997, *J. phys. Chem.*, **1010**, 6504.
[20] Qian, J., Green, R. J., and Anderson, S. L., 1998, *J. chem. Phys.*, **108**, 7173.
[21] Conaway, W. E., Morrison, R. J. S., and Zare, R. N. 1985, *Chem. Phys. Lett.*, **113**, 429.
[22] Conaway, W. E., Ebata, T., and Zare, R. N., 1987, *J. chem. Phys.*, **87**, 3453.
[23] Conaway, W. E., Ebata, T., and Zare, R. N., 1987, *J. chem. Phys.*, **87**, 3447.
[24] Ebata, T. and Zare, R. N., 1986, *Chem. Phys. Lett.*, **130**, 467.
[25] Guettler, R. D., Jones, G. C., Jr, Posey, L. A., and Zare, R. N., 1994, *Science*, **266**, 259.
[26] Guettler, R. D., 1995, PhD Thesis, Stanford University.
[27] Jones, G. C., Jr, 1996, PhD Thesis, Stanford University.
[28] Gerlich, D., and Rox, T,. 1989, *Z. Phys.* D, **13**, 259.
[29] Gerlich, D., and Kaffer, G., 1989, *Astrophys. J.*, **347**, 849.
[30] Gerlich, D., 1993, *J. chem. Soc., Faraday Trans.*, **89**, 2199.
[31] Shao, J. D., Li, Y. G., Flesch, G. D., and Ng, C. Y., 1987, *J. chem. Phys.*, **86**, 170.
[32] Liao, C. L., Xu, R., Flesch, G. D., Baer, M., and Ng, C. Y., 1990, *J. chem. Phys.*, **93**, 4818.
[33] Shao, J. D., and Ng, C. Y., 1986, *J. chem. Phys.*, **84**, 4317.
[34] Metayer-Zeitoun, C., Alcarez, C., Anderson, S. L., Palm, H., and Dutuit, O., 1995, *J. phys. Chem.*, **99**, 15 523.
[35] Palm, H., Berthomieu, D., Metayer-Zeitoun, C., Alcarez, C., and Dutuit, O., 1994, *Proceedings of Symposium on Atomic and Surface Physics '94*, pp. 180–183.
[36] Dutuit, O., Palm, H., Berthomieu, D., and Herman, Z., 1996, *Chem. Phys.*, **209**, 259.
[37] Zhu, L., and Johnson, P., 1991, *J. chem. Phys.*, **94**, 5769.
[38] Ashfold, M. N., Tutcher, B., Yang, B., Jin, Z., and Anderson, S. L., 1987, *J. chem. Phys.*, **87**, 5105.

[39] ORLANDO, T. M., ANDERSON, S. L., APPLING, J. R., and WHITE, M. G., 1987, *J. chem. Phys.*, **87**, 852.
[40] YANG, B., ESLAMI, M. H., and ANDERSON, S. L., 1988, *J. chem. Phys.*, **89**, 5527.
[41] KIM, H.-T., and ANDERSON, S. L., 2001, *J. chem. Phys.*, **114**, 3018.
[42] LIU, J., and ANDERSON, S. L., 2001, *J. chem. Phys.* (in the press).
[43] GERLICH, D., 1992, *Adv. chem. Phys.*, **82**, 1.
[44] FISK, G. A., MCDONALD, J. D., and HERSCHBACH, D. R., 1967, *Discuss. Faraday Soc.*, **44**, 228.
[45] FRISCH, M. J., TUCKS, G. W., SCHLEGEL, H. B., SCUSERIA, G. E., ROBB, M. A., CHEESEMAN, J. R., ZAKRZEWSKI, V. G., MONTGOMETRY, J. A., STRATMANN, R. E., BURANT, J. C., DAPPRICH, S., MILLAM, J. M., DANIELS, A. D., KUDIN, K. N., STRAIN, M. C., FARKAS, O., TOMASI, J., BARONE, V., COSSI, M., CAMMI, R., MENNUCCI, B., POMELLI, C., ADAMO, C., CLIFFORD, S., OCHTERSKI, J., PETERSON, G. A., AYALA, P. Y., CUI, Q., MOROKUMA, K., MALICK, D. K., RABUCK, A. D., RAGHAVACHARI, K., FORESMAN, J. B., CIOSLOWSKI, J., ORITZ, J. V., STEFANOV, B. B., LIU, G., LIASHENKO, A., PISKORZ, P., KOMAROMI, I., GOMPERTS, R., MARTIN, R. L., FOX, D. J., KEITH, T., AL-LAHAM, M. A., PENG, C. Y., NANAYAKKARA, A., GONZALEZ, C., CHALLACOMBE, M., GILL, P. M. W., JOHNSON, B. G., CHEN, W., WONG, M. W., ANDRES, J. L., HEAD-GORDON, M., REPLOGLE, E. S., and POPLE, J. A., 1998, *GAUSSIAN 98* (Pittsburgh, Pennsylvania: Gaussian, Inc.).
[46] ZHU, L., and HASE, W. L., *Quantum Chemistry Program Exchange QCPE 644*.
[47] LIAS, S. G., BARTMESS, J. E., LIEBMAN, J. F., HOLMES, J. L., and Levin, R. D., 1988, *J. phys. Chem. Ref. Data*, **17**, suppl. 1.
[48] KLIPPENSTEIN, S. J., 1996, *J. chem. Phys.*, **104**, 5437.
[49] YI, M., and SCHEINER, S., 1996, *Chem. Phys. Lett.*, **262, 567.**
[50] TROE, J., 1985, *Chem. Phys. Lett.*, **122**, 425.
[51] LIAS, S. G., LIEBMAN, J. F., and LEVIN, R. D., 1984, *J. phys. Chem. Ref. Data*, **13**, 695.
[52] HUNTER, E. P., and LIAS, S. G., 1998, *J. phys. Chem. Ref. Data*, **27**, 413.
[53] DETURI, V. F., and ERVIN, K. M., 1998, *Int. J. Mass Spectrom. Ion Processes*, **175**, 123.
[54] MATSUMOTO, A., OKADA, S., TANIGUCHI, S., and HAYAKAWA, T. 1975, *Bull. chem. Soc. Japan*, **48**, 3387.
[55] ADAMS, N. G., SMITH, D., and PAULSON, J. F., 1980, *J. chem. Phys.*, **72**, 288.
[56] THOMAS, R., BARASSIN, J., and BARASSIN, A., 1981, *Int. J. Mass Spectrom. Ion Phys.*, **41**, 95.